Stroke

BASIC AND TRANSLATIONAL SCIENCES

CD31 Mimetic Coating Enhances Flow Diverting Stent Integration into the Arterial Wall Promoting Aneurysm Healing

Jonathan Cortese, MD*; Charlotte Rasser, PhD*; Guillaume Even, BSc; Sylvia M. Bardet, PhD; Christine Choqueux, BSc; Jules Mesnier, MD; Marie-Laure Perrin, MD; Kevin Janot, MD; Jildaz Caroff, MD, PhD; Antonino Nicoletti, PhD; Jean-Baptiste Michel, MD, PhD; Laurent Spelle, MD, PhD; Giuseppina Caligiuri, MD, PhD; Aymeric Rouchaud, MD, PhD†

BACKGROUND AND PURPOSE: Beyond aneurysmal occlusion, metallic flow diverters (FDs) can induce an adverse endovascular reaction due to the foreignness of metal devices, hampering FD endothelialization across the aneurysm neck, and arterial healing of intracranial aneurysms. Here, we evaluated the potential benefits of an FD coating mimicking CD31, a coreceptor critically involved in endothelial function and endovascular homeostasis, on the endothelialization of FDs implanted in vivo.

METHODS: Nitinol FD (Silk Vista Baby) and flat disks were dip-coated with a CD31-mimetic peptide via an intermediate layer of polydopamine. Disks were used to assess the reaction of endothelial cells and blood elements in vitro. An aneurysm rabbit model was used to compare in vivo effects on the arterial wall of CD31-mimetic–coated (CD31-mimetic, n=6), polydopamine-coated (polydopamine, n=6), and uncoated FDs (bare, n=5) at 4 weeks post-FD implantation. In addition, long-term safety was assessed at 12 weeks.

RESULTS: In vitro, CD31-mimetic coated disks displayed reduced adhesion of blood elements while favoring endothelial cell attachment and confluence, compared to bare and polydopamine disks. Strikingly, in vivo, the neoarterial wall formed over the CD31-mimetic-FD struts at the aneurysm neck was characteristic of an arterial tunica media, with continuous differentiated endothelium covering a significantly thicker layer of collagen and smooth muscle cells as compared to the controls. The rates of angiographic complete occlusion and covered branch arterial patency were similar in all 3 groups.

CONCLUSIONS: CD31-mimetic coating favors the colonization of metallic endovascular devices with endothelial cells displaying a physiological phenotype while preventing the adhesion of platelets and leukocytes. These biological properties lead to a rapid and improved endothelialization of the neoarterial wall at the aneurysm neck. CD31-mimetic coating could therefore represent a valuable strategy for FD biocompatibility improvement and aneurysm healing.

GRAPHIC ABSTRACT: An online graphic abstract is available for this article.

Key Words: endothelial cells ■ homeostasis ■ intracranial aneurysms ■ leukocytes ■ platelet ■ polydopamine ■ stent

Flow diverters (FDs) have provided a paradigm shift for endovascular reconstructive treatment of cerebral aneurysms.[1,2] These metal stents aim at (1) reducing the entering blood flow, redirecting it into the parent artery and (2) promoting aneurysm sac sealing and subsequent occlusive thrombus formation.[1] However, FD use is hampered by the life-threatening occurrence of thrombotic or hemorrhagic complications.[2,3] Indeed, in 20.1% of cases,

Correspondence to: Aymeric Rouchaud, MD, PhD, University of Limoges, XLIM UMR CNRS 7252, France, Email aymeric.rouchaud@gmail.com or Giuseppina Caligiuri, MD, PhD, Laboratory for Vascular Translational Science, Université de Paris, INSERM U1148, France, Email giuseppina.caligiuri@inserm.fr

*Drs Cortese and Rasser are co-first authors.

†Drs Caligiuri and Rouchaud are co-last authors.

The Data Supplement is available with this article at https://www.ahajournals.org/doi/suppl/10.1161/STROKEAHA.120.030624.

For Sources of Funding and Disclosures, see page 685.

Stroke is available at www.ahajournals.org/journal/str

Nonstandard Abbreviations and Acronyms

APC	allophycocyanin
aSMA	alpha smooth muscle actin
EC	endothelial cell
ECM	extracellular matrix
FD	flow diverter
VE-cadherin	vascular endothelial cadherin

FD-induced aneurysm occlusion fails, with a perioperative morbidity-mortality rate of 7.1%.[4] Delayed aneurysm rupture thus remains a major concern due to its severity.[3] This presumably involves proteolytic activity of the intraaneurysmal thrombus, aneurysmal flow persistence, as well as inflammation inherent to metal struts.[5,6] Furthermore, due to the risk of thromboembolic complications, dual antiplatelet therapy before FD implantation is mandatory, increasing the risk of hemorrhagic complications.[7]

A recent report points at the endothelialization across the aneurysm neck as the critical step for curing intracranial aneurysm through FD implantation.[8] Indeed, the growth and function of endothelial cells (ECs) over the healing thrombus, across the aneurysm neck, may be hampered by the adverse endovascular reaction to the foreignness of the metallic device. Therefore, promoting rapid FD colonization by differentiated ECs forming physiological adherens junctions (ie, expressing VE-cadherin [vascular endothelial cadherin] and CD31 at the lateral cell-cell borders)[9] could represent a valuable strategy improving FD biocompatibility and aneurysm healing.

CD31 is a transmembrane glycoprotein expressed constitutively and exclusively on platelets, leukocytes, and ECs.[10] It plays a major role in maintaining circulation homeostasis.[11] Importantly, a synthetic CD31-mimetic peptide, derived from the juxtamembrane extracellular CD31 sequence, mimicking CD31 functions, has recently been shown to promote arterial healing.[12] Thus, this CD31-mimetic peptide represents an ideal candidate to enhance FD integration in the arterial wall, preventing stent-induced inflammation and thrombosis. Indeed, coating FDs with a CD31-mimetic peptide could reduce the adverse reactivity of strut-adjacent ECs as well as blood flowing platelets and leukocytes.

To test this, we investigated the effect of FD CD31-mimetic coating first in vitro by assessing the reaction of blood elements and ECs in contact with CD31-mimetic coated disks. Second, to analyze FD endothelialization and neoarterial wall formation in vivo, we implanted CD31-mimetic-FDs in the rabbit elastase saccular aneurysm model which has histological, morphological, biological, and hemodynamic similarities with the human pathology.

METHODS

The data that support the findings of this study are available from the corresponding author upon reasonable request.

Surface Functionalization and Peptide Grafting

Following the procedure from patent file PCT/FR 2018/052991, the CD31-mimetic peptide was modified to be covalently immobilized by strain-promoted alkyne—azide cycloaddition reaction onto nitinol disks (0.48 mm in diameter, 0.25 mm thick, water-jet cut, and polished from flat nitinol bands: Cust PO 2015012386, Fort Wayne Metals, Ireland/Vuichard, Dingy en Vuache, France) and onto FDs (Silk Vista Baby, diameter 3.25 mm×15 mm, from Balt Extrusion, Montmorency, France).

Briefly, biorthogonal covalent grafting of an azide derivative of CD31-mimetic peptide onto nitinol surfaces (flat disks and FDs) was obtained via 3 successive dip-coating steps, under sterile conditions. Nitinol samples were immersed individually in an alkaline solution of dopamine (Alfa Aesar no. A11136, dissolved at 2 mg/mL in tris buffer, pH 8.5) for 22 hours, under stirring, to obtain a polydopamine layer.[13] Soluble oxidized polydopamine was carefully removed by extensive washes in sterile water and the polydopamine-coated disks were submitted to a second dip-coating step to graft an amine-functionalized cyclooctyne derivative anchor arm (BCN-amine, Sigma no. 745073) onto the free catechol groups of the polydopamine layer (0.1 mg/ml in tris buffer, pH 8.5) under stirring for 22 hours.[14] After extensive washing, the disks were immersed in the peptide solution (CD31-mimetic-azide, 50 µM in sterile water) and allowed to react for 30 minutes, under stirring.

As polydopamine may itself have a biological response, we used both bare-metal and polydopamine-coated samples as control groups for all experiments; bare refers to bare/unmodified nitinol surfaces, polydopamine refers to polydopamine coating alone, and CD31-mimetic refers to CD31-mimetic peptide coating onto an intermediate layer of polydopamine.

Reaction of Blood Elements and Arterial ECs In Vitro

CD31-mimetic and control nitinol disks were immersed and allowed to react for 1 hour at 37 °C under stirring (400 RPM) in whole peripheral venous blood withdrawn in PPAK (D-phenylalanyl-N-[(1S)-4-[(aminoiminomethyl)amino]-1-(2-chloroacetyl)butyl]-L-prolinamide) trifluoroacetate salt–containing tubes. The presence of stably adherent blood elements onto the surface of the washed samples was qualitatively evaluated by immunofluorescence microscopy.

Primary human coronary artery ECs (Lonza) were expanded in culture flasks coated with 100 µg/mL of type 1 collagen (Thermo Fisher Scientific) in EC Growth medium (EGM-2 MV, Lonza) supplemented with 15% FBS (Gibco). The cells were used between passages 3 and 5. Coated and uncoated metal disks were placed in 96-well plates before the addition of 100 000 ECs suspended in 100 µL of their growth medium. After a 48 hour incubation at 37 °C and 5% CO_2, the adherent cells were processed for immunocytofluorescence microscopy.

Stroke. 2021;52:677–686. DOI: 10.1161/STROKEAHA.120.030624

Immunofluorescence Microscopy and Quantitative Analysis

Adherent platelets were revealed on blood-contacted nitinol disks after extensive washing using a CD41/CD63 targeting monoclonal antibody coupled to fluorescein isothiocyanate (FITC; no. 130-109-423). Bound erythrocytes were detected with a monoclonal APC (allophycocyanin)-conjugated mouse anti-human glycophorin A antibody (CD235a, no. 130-118-356, both from Miltenyi Biotech). Human coronary artery EC–contacted disks were processed using a monoclonal mouse anti-human CD31 antibody (no. M0823, Dako; revealed with AlexaFluor488 secondary antibody) and a polyclonal rabbit anti-human VE-Cadherin (no. ab33168, Abcam; revealed with a rhodamine-conjugated secondary antibody). Nuclei were stained with DAPI and samples mounted with ProlongGold. Images were taken with an Axio Observer fluorescence microscope (Zeiss) equipped with an ORCA II Digital CCD camera (Hamamatsu Photonics).

Images from fluorescence microscopy were used for quantification using Image J (National Institutes of Health) software, v1.50i for MacOS, with the "analyze particles" command. Erythrocytes, platelets, and leukocytes were counted on blood-contacted disk (data expressed as N/mm^2). Adherent ECs were analyzed both in terms of number and functional differentiation, by measuring the signal integrated density of immunostained CD31 and VE-cadherin at the lateral junctions.

Animal Care

We used White New Zealand male rabbits, weight 3.0 to 3.5 kg. Food and water were provided ad libitum. All animal care and experimental procedures were conducted in accordance with the 2013 French legislation and European Community guidelines (directive 2010/63/UE for the Care and Use of Laboratory Animals). The study received approval from the regional Ethical and Animal Care Committee (APAFIS no. 5747-2018022812464127). For each procedure, general anesthesia was obtained using intramuscular injection of 0.5 mg/kg of Acepromazine (Vetranquil 1%), 20 mg/kg of Ketamine, and 4.5 mg/kg of Xylazine (Rompun). Postoperative analgesia was assured with Buprenorphine 0.02 to 0.04 mg/kg per 6 hours IM administrated with pain systematic evaluation before and after the administration. Animals were euthanized under general anesthesia during the last procedure using a lethal injection of pentobarbital (60 mg/kg) followed with bilateral thoracotomy.

FD Implantation and Angiographic Evaluation

Aneurysm creation procedures were performed as previously described.[15] Elastase-induced aneurysms were created in 18 rabbits (6 per group). Aneurysms were treated 3 weeks after aneurysm creation. Two days before FD implantation, subjects were premedicated with aspirin (10 mg/kg PO), this medication regimen was continued until the final procedure. All endovascular procedures were performed with the Mobil C-arm–BV Endura (Philips Medical Systems).

Rabbits were randomized in 3 different experimental groups: the bare group was implanted with bare Silk Vista Baby FDs (bare-FD n=6), the polydopamine group with Silk Vista Baby FDs coated with polydopamine alone (polydopamine-FD, n=6), and the CD31-mimetic group with Silk Vista Baby FDs coated with the CD31-mimetic peptide (CD31-mimetic-FD, n=6; Figure IA and IB in the Data Supplement).

FD endothelialization and patency of covered branches were also analyzed using a second FD, with the same surface modification as the first one (bare-FD, polydopamine-FD or CD31-mimetic-FD), placed in the abdominal aorta across the origin of at least one pair of lumbar arteries in 6 subjects (2 from each group).

Half the subjects were followed for 4 weeks for histopathologic comparison (including all subjects with FDs implanted in the abdominal aorta) and half were followed for 12 weeks for safety evaluation. At the time of euthanization, digital subtraction angiography of the aortic arch (and the abdominal aorta when necessary) was performed. Aneurysm occlusion was noted for all subjects using a 3-point scale, including grade 1, complete occlusion; grade 2, near-to-complete occlusion; and grade 3, incomplete occlusion. Patency of stented covered branch arteries, including lumbar and vertebral arteries was also evaluated. Harvested aneurysms and aorta segments were immediately fixed in 4% paraformaldehyde and in 2.5% glutaraldehyde, respectively.

Histopathology

After 48 hours of paraformaldehyde fixation, explanted aneurysms at 4 weeks were embedded in a poly-(methyl-methacrylate) PMMA resin, then sectioned transversally (8 µm section) in a microtome equipped with a tungsten carbide blade (Figure IC and ID in the Data Supplement). Images from stained slides were numbered with Hamamatsu Nanozoomer 2.0RS (Hamamatsu Photonics) and an Axio Observer fluorescence microscope (Zeiss) equipped with an ORCA II Digital CCD camera (Hamamatsu Photonics).

Tissue morphology across the aneurysm neck was qualitatively assessed on microscopic slides stained with Picro Sirius Red and Carstairs staining as well as by immunofluorescent detection of aSMA (alpha smooth muscle actin) using a primary mouse anti-human monoclonal antibody (clone 1A4, Sigma) and a Cy3 goat anti-mouse IgG secondary antibody (Jackson Immunoresearch).

Digital images of Picro Sirius Red–stained slides acquired in the green and red fluorescent channels were used for quantitative analysis of neoarterial thickness around the FD struts at the level of the aneurysm neck as previously described,[16] running a custom macro written in Quips language (QWin software, Leica) on 3 distinct histological sections for each aneurysm.

Scanning Electron Microscopy and Multiphoton Microscopy

Explanted aortic vessels were cut longitudinally into 2 parts to expose the luminal surface. The half containing the lumbar arteries was processed for conventional scanning electron microscopy. Conventional scanning electron microscopy was performed using Philips XL30 ESEM FEG microscope.

The other half of the aorta was processed for multiphoton microscopy performed with a customized multiphoton microscope BX61WI/FV1200MPE (Olympus) coupled with a tuneable femtosecond Ti:Sapphire pulsed laser (Chameleon Ultra II, Coherent), as previously described.[17] This technique allows

a higher penetration depth in the neoarterial tissue covering the device (400 µm maximum) with high-resolution 3-dimension reconstructed images. Seven to 10 random zones of each stent, excluding 2.5 mm at the distal and proximal ends, were imaged. Collagen quantification, ECM (extracellular matrix) thickness measurement, tissue architecture evaluation, and 3-dimension fiber orientation measurements were assessed by second harmonic generation signal in a 3-dimension stack after z-projection. Collagen fiber orientation was calculated using the OrientationJ plugin (ImageJ [National Institutes of Health] software). Collagen area (%) was quantified with the analyze particles command.

Statistical Analysis

Data are presented as mean±SD. The Kruskal-Wallis test with Dunn post-test was used for skewed data. Normally distributed variables were analyzed with 1-way ANOVA with Bonferroni post hoc F. The Fisher exact test with Bonferroni correction for multiple tests was used for comparison of nominal variables. All statistical calculations were performed with R software (R-3.6.1). Differences were considered statistically significant at the $P<0.05$ level.

RESULTS

Interaction of Blood Elements and ECs With Experimental Nitinol Disks

Erythrocyte and platelet coverage was barely visible and significantly reduced on CD31-mimetic disks compared with polydopamine and bare nitinol disks (Kruskal-Wallis $\chi^2[2]$; $P<0.0001$ for both erythrocytes and platelets; Figure 1). Very few leukocytes were discernible on all 3 surfaces (Kruskal-Wallis $\chi^2[2]$; $P=0.1$).

Adhering EC density was similar in the 3 groups (nuclei N/mm^2, Kruskal-Wallis $\chi^2[2]$; $P=0.12$) but the integrated density of CD31 and VE-cadherin signal was significantly increased on CD31-mimetic as compared to polydopamine and bare surfaces (Kruskal-Wallis $\chi^2(2)$; $P=0.001$ and $P=0.007$ for CD31 and VE-cadherin, respectively; Figure 2). Altogether these results suggest that CD31-mimetic coating decreases erythrocyte and platelet accumulation on metal surfaces while improving differentiated EC colonization in vitro.

Aneurysm Sizes and Angiographic Results

Induced aneurysms were of equivalent sizes in all 3 groups (Table 1). One rabbit died of infection during the first week after FD implantation in the bare group and was thus excluded from the analyses. One animal in the 12 weeks polydopamine group was sacrificed at 4 weeks because of a right upper leg deficit (due to stent occlusion). Grade 1 occlusion rates were noted in 3 (60%), 4 (66%), and 5 (82%) aneurysms in the bare, polydopamine, and CD31-mimetic group respectively ($P=0.8$; Table 1). The remaining aneurysms were not occluded with grade 3 occlusion. In the polydopamine group, 2 stents spontaneously occluded at 4 weeks despite antiplatelet regimen (only one symptomatic). All other parent, vertebral and lumbar arteries remained patent without stenosis.

Effect of CD31-Mimetic-FDs on Neoarterial Formation at Aneurysm Sites

Histological analysis of the arterial wall covering the FD struts at the neck of aneurysmal sacs revealed striking differences for each condition (Figure 3A). In the bare-FD condition, the struts were covered by a thin, barely existent, disorganized neointima, devoid of smooth muscle cells and containing no detectable collagen. Further analysis revealed that the neoarterial wall was composed of fibrin and erythrocytes, with complete absence of ECs at the luminal border of bare-metal FDs, reminiscent of a fresh clot. In contrast, CD31-mimetic-FD struts were covered by a thick, organized neointima, with layers of mesenchymal and smooth muscle cells (expressing aSMA), oriented sheets of collagen and elastin in the ECM, and a continuous endothelial monolayer. This organization was observed both at the aneurysm neck, completely covered by a neoarterial wall, and away from it. Concerning polydopamine coating, the results were inconsistent, with 2 intrastent occlusions, one case of neointimal excessive hyperplasia, and one case with poor neointimal formation (discussed below). Histological analysis of the hyperplasia case indicated that the ECs covering the polydopamine-coated FD were layered onto a thick neointima composed of abundant and undifferentiated mesenchymal cells, largely lacking aSMA, in direct contact with the luminal border (Figure 3A).

Quantitative morphometry analyses confirmed that the thickness of the neoarterial wall at the neck of experimental aneurysms was similarly higher in aneurysms implanted with coated FDs (50.4±24 µm in polydopamine and 42.9±25 µm in CD31 mimetic, $P=1$) as compared to what we observed with bare-metal devices (25.5±12 µm in Bare; $P=0.004$ versus polydopamine and $P=0.019$ versus CD31-mimetic; Figure 3B). Although measuring the neointima thickness indicated no significant difference between the bare and CD31-mimetic–coated FDs, it revealed that CD31 coating reduced neointimal thickness as compared to the measured polydopamine case. Altogether these results suggest that CD31-mimetic coating promotes physiological neoarterial wall formation.

Effect of CD31-Mimetic Coating on FDs Implanted at Abdominal Aortic Sites

Collagen thickness, FD endothelialization, and patency of covered branches were analyzed 4 weeks post-FD implantation in the aortic sites. Quantification of collagen

 Stroke. 2021;52:677–686. DOI: 10.1161/STROKEAHA.120.030624

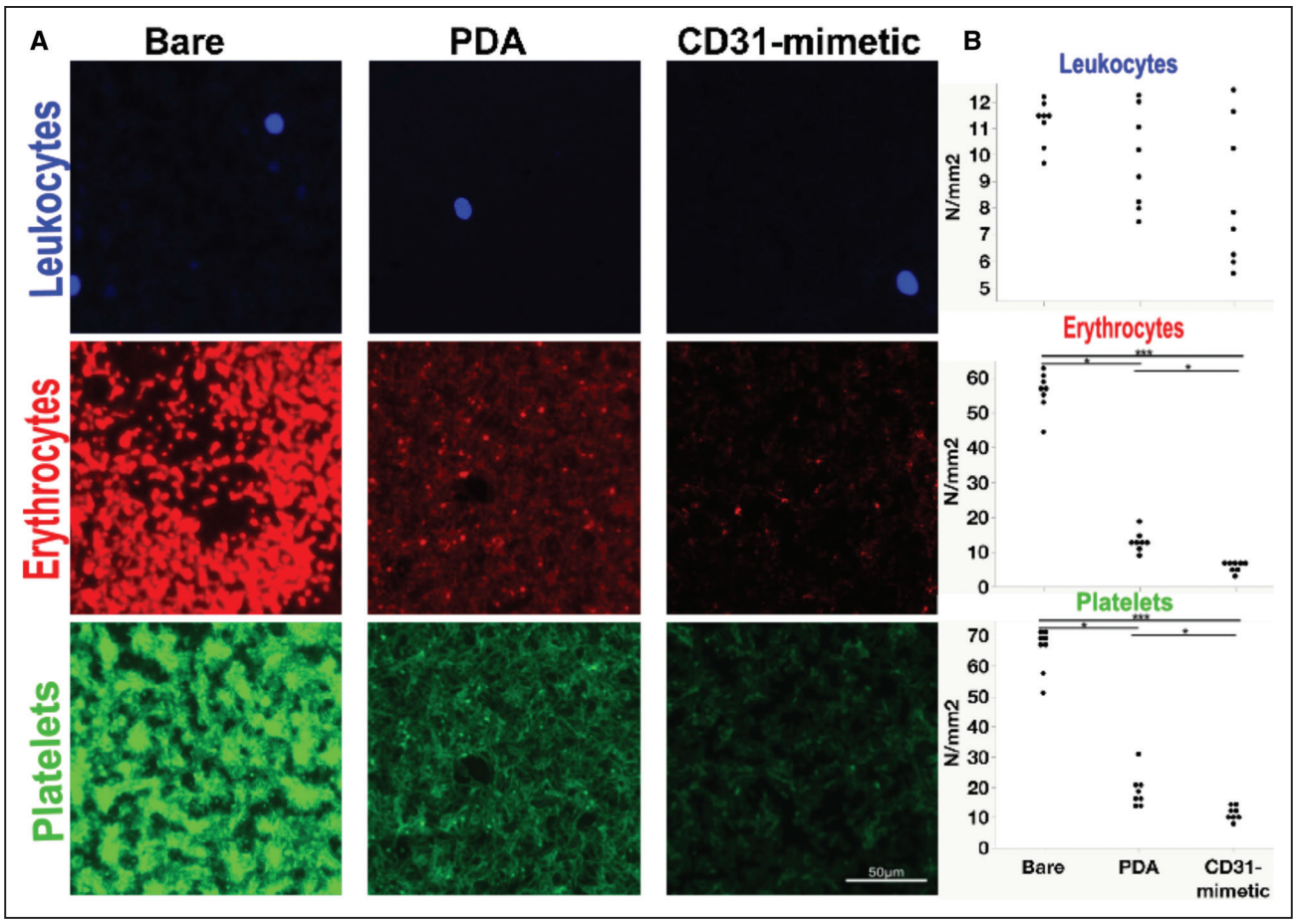

Figure 1. Representative fluorescence micrographs of bare, polydopamine (PDA), and CD31-mimetic nitinol disks after 1-h incubation in whole blood at 37°C under stirring and quantitative automated analysis.
A, Green fluorescence: adherent platelets (CD41/CD63). Red fluorescence: Adherent erythrocytes (glycophorin A). Blue fluorescence: Leukocytes via the presence of a 4',6-diamidino-2-phenylindole (DAPI)+element. **B**, quantification of leukocytes, erythrocytes, and platelets (N/mm^2, Kruskal-Wallis with Dunn post-test: **P*<0.05, ****P*>0.001).

tissue thickness over the FD struts using multiphoton microscopy indicated that ECM thickness was significantly higher in the CD31-mimetic condition compared with the controls (CD31-mimetic [n=20] versus polydopamine [n=20] *P*<0.005, CD31-mimetic versus bare [n=14] *P*<0.001, and polydopamine versus bare *P*<0.005; after One-way ANOVA with Bonferroni post hoc F[2,52]=22.02, *P*<0.05).

Furthermore, consistent with our previous observations, CD31-mimetic-FD struts displayed an organized ECM with a lower fiber dispersion as compared to both polydopamine and bare-FD struts (Figure 4, Figures III and IV and Movies I and II in the Data Supplement). Using scanning electron microscopy, we observed a velvet cover reminiscent of a continuous cell layer overall 3 types of FD struts implanted in the lumbar arteries. Importantly though, ostia of the covered lumbar arteries were patent in all 3 conditions with no significant intimal growth over the struts (Figure II in the Data Supplement). Altogether these results indicate that CD31-coating onto metal struts both promotes physiological ECM organization within the arterial wall covering the metal struts and avoids arterial branch occlusion, ensuring covered branch arterial patency.

DISCUSSION

Here, we show that CD31-mimetic coating reduces blood element reaction and increases EC adhesion in vitro and enhances neoarterial wall formation in vivo. Thus, our data strongly suggest that CD31-mimetic coating is in favor of aneurysm healing. The presence of the CD31-mimetic peptide likely acts as a CD31 agonist, the role of which is to sustain EC survival and barrier function.[18] Indeed, we observed a higher rate of organized neoartery wall with continuous endothelium, thicker ECM, and high density of oriented collagen.

Arterial wall reconstitution is essential as FD healing is strongly correlated with aneurysm occlusion.[8,19] Also, the tightness of this biological barrier and the timing of its reconstitution, both improved with the use of CD31-mimetic coating, are crucial to prevent delayed rupture

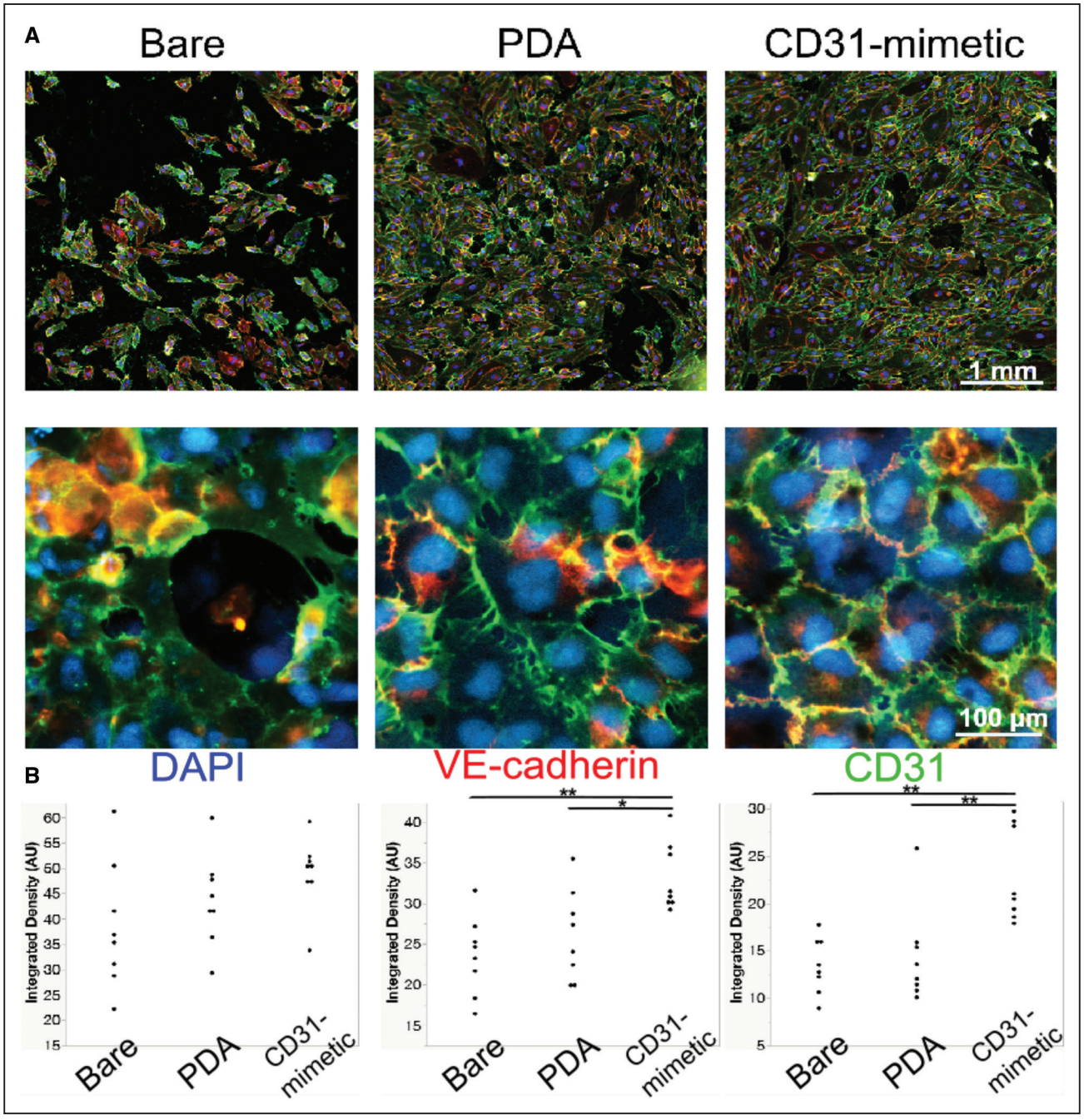

Figure 2. Representative fluorescence micrographs of bare, polydopamine (PDA), and CD31-mimetic nitinol disks after 48 h of endothelial cell incubation and quantitative automated analysis.
A, Green fluorescence: CD31. Red fluorescence: VE-Cadherin (vascular endothelial cadherin). Blue fluorescence: 4',6-diamidino-2-phenylindole (DAPI). First row: low magnification. Second and third rows: higher magnifications. **B**, quantification of CD31, VE-cadherin, and DAPI (integrated density, Kruskal-Wallis with Dunn post-test: *P<0.05, **P>0.01).

after FD implantation.[3] The faster establishment of an impermeable barrier prevents the biological cascade induced by acute aneurysmal thrombosis, likely responsible for metallopeptidase activation and intra-aneurysmal fibrinolysis.[20,21] The use of biologically improved FDs with accelerated healing and faster exclusion of the aneurysm is of the uttermost importance since actual recommendations, like associated coiling, fail to prevent aneurysm stabilization and delayed ruptures.[3]

As the CD31-mimetic-FD stimulates neointimal growth, it was necessary to evaluate if the patency of such covered branch arteries was altered. In our study, we observed excellent patency of branch arteries covered by CD31-mimetic-FDs. This could be linked to continuous high blood flow inhibiting endothelial growth. Conversely, initial low blood flow over the CD31-mimetic-FD in the aneurysm sac likely permits stimulation of neointimal formation at the neck of the aneurysm and thus efficient healing.[22]

Stroke. 2021;52:677–686. DOI: 10.1161/STROKEAHA.120.030624

Table. Aneurysm Size (mm, Mean±SD) and Angiographic Results

	Group			
	Bare	PDA	CD31-mimetic	*P* value
Aneurysm size, mm				
Height	6.9±2.8	9.0±4.2	7.1±3.1	0.51
Width	3.2±0.6	3.3±0.2	3.1±0.5	0.68
Neck	5.6±2.0	4.8±1.3	4.1±1.2	0.85
Occlusion rate				
4 wk	2/2	2/4*	2/3	
12 wk	1/3	2/2	3/3	
Total	3/5 (60%)	4/6 (66%)	5/6 (83%)	0.8
Lumbar artery patency	2/2	2/2	2/2	1

FD indicates flow diverter; and PDA, polydopamine.
*2 PDA-coated FDs presented intrastent thrombosis.

In agreement with its recently documented proadhesive properties,[23] polydopamine coating showed a detectable increase of EC adhesion in vitro. However, quantification of CD31 and VE-cadherin expression at the lateral junctions clearly showed a more differentiated phenotype of cells adhering onto CD31-mimetic surfaces compared to polydopamine surfaces. Furthermore, our in vivo experiments document a consistent CD31-mimetic effect with the formation of a well-structured neoarterial wall across the aneurysm neck. Instead, divergent effects with 2 intrastent occlusions were observed in the polydopamine condition. These results cannot enable us to conclude on the effect of polydopamine coating in vivo on such a small number of cases. Nevertheless, the presence of free charged groups (catechol and amine) on the polydopamine coating could induce local platelet and leukocyte activation,[24] driving increased smooth muscle cell proliferation and neointimal growth in response to aneurysm induction, as observed. Of note, the effect of polydopamine coating appeared more consistent in the aortic site. FD implantation within a healthy artery might induce a less drastic remodeling response as compared to implantation at a pathological aneurysm site, hence

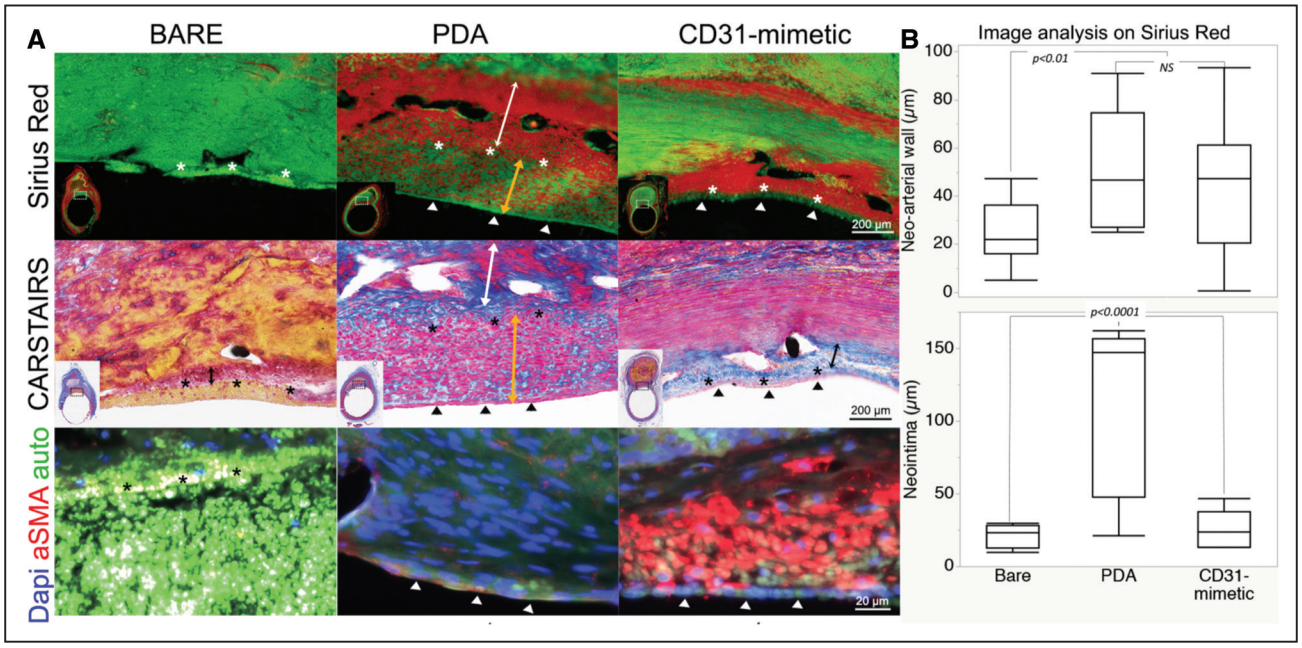

Figure 3. Representative histological sections with various stainings for neoarterial wall and neointima qualitative and quantitative analysis at the neck of occluded aneurysms 4 wk after flow diverter (FD) implantation.
A, **Top**, Picro Sirius Red staining revealing collagen (red). Green is due to autofluorescence. The asterisks in the **top** and **middle** parts mark the luminal limit of the ECM (extracellular matrix)-rich layer (ie, the internal elastic lamina of the neoarterial walls) in all 3 conditions. In the polydopamine (PDA) and CD31-mimetic conditions, arrowheads point at a continuous endothelium lining the arterial lumen (see **middle**). **Middle**, Results of staining with Carstairs staining. The orange-red coloration in the bare condition reveals fibrin and erythrocytes. In the PDA and CD31-mimetic conditions, the pink cellular layer lining the inner side of the arterial wall (arrowheads as in the **top**) indicates the presence of a continuous endothelium. Blue reveals collagen/ECM. In the CD31-mimetic condition, the pink coloration in the neointima reveals smooth muscle cells, as documented by the immunofluorescent detection of aSMA (alpha smooth muscle actin; see **lower**), distributed in between ECM fibers parallel to the arterial wall, reminiscent of an arterial tunica media. The endothelial cell layer is directly in contact with these cells, reflecting the absence of a neointima. In contrast, in the selected PDA sample, the pink coloration in the most inward cellular layer reveals a mass of aSMA-negative mesenchymal cells, indicative of thick neointima formation. In the **top** and **middle**, double arrows represent the mean for each quantitative analysis (neoarterial wall thickness: white double arrow; ECM/neointima thickness: orange double arrow; **B**). **Bottom**, Immunofluorescent detection of aSMA (red) and nuclei (4',6-diamidino-2-phenylindole [DAPI], blue). Green reflects aldehyde-fixation–driven autofluorescence of red blood cells and structural elements, such as collagen and elastin. Note the absence of specific aSMA staining in the PDA condition. **B**, Quantitative analysis of neoarterial (**top**) and neointimal (**bottom**) thickness at the aneurysm neck in all 3 conditions. Neoarterial wall thickness mean±SD were 50±24 µm in PDA, 43±25 µm in CD31 mimetic, and 25±12 µm in bare; *P*=0.004 versus PDA and *P*=0.019 versus CD31-mimetic). Neointima thickness mean±SD were: 20.6±84 µm in Bare; *P*=0.004 versus PDA and *P*=0.019 versus CD31-mimetic; 111±61 µm in PDA, 25±12 µm in CD31 mimetic (*P*=1).

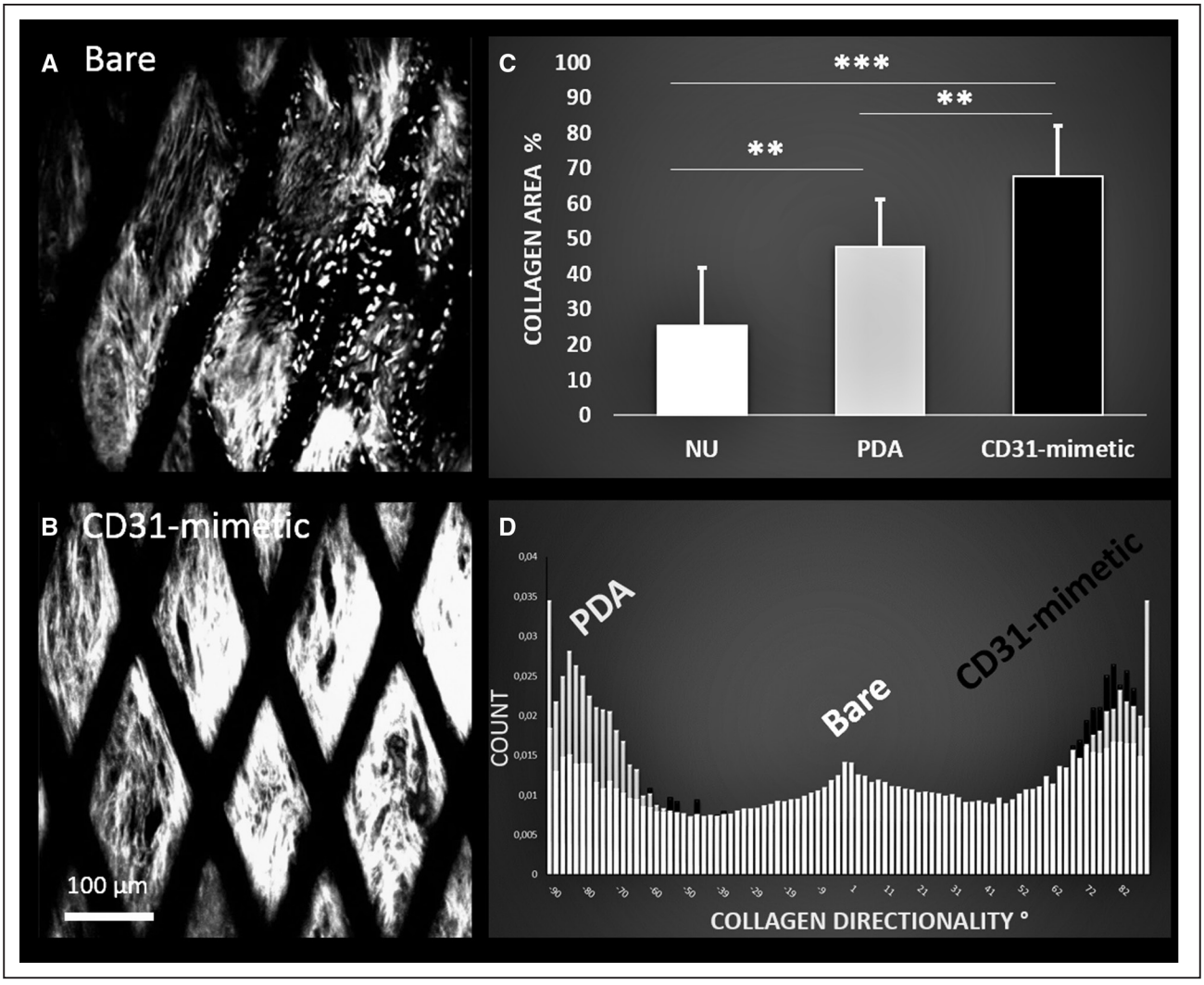

Figure 4. Representative multiphoton microscopy based on second harmonic generation signal photographs, quantification of collagen fibers, and collagen fiber dispersion 4 wk after flow diverter (FD) implantation in rabbit aortas.
A, Bare-FD. **B**, CD31-mimetic-FD (P8RI). **C**, CD31-mimetic, and polydopamine (PDA) FD present a thicker collagen ECM (extracellular matrix) compared with bare, CD31-mimetic-FD displaying the highest rate of collagen (mean±SEM, 1-way ANOVA with Bonferroni post-test: $^{**}P<0.005$ and $^{***}P<0.001$). **D**, Collagen fiber orientation measurements show an overall lower fiber dispersion with PDA and CD31-mimetic compared to the bare-FD. Colored figures with multiphoton microscopy are available in the Data Supplement.

the more consistent effect of polydopamine coating in the lumbar artery. All the same, our results indicate that, within a healthy artery, polydopamine coating alone induces the formation of a thinner and less organized ECM as compared to CD31-mimetic coating. The addition of CD31-mimetic peptide likely has a double effect: (1) it masks the free catechol and amine groups reducing the nonspecific interaction of polydopamine with surrounding cells, allowing a consistent CD31-specific response and (2) it increases FD biocompatibility thanks to the homophilic interaction between the CD31-mimetic peptide and the endogenous CD31 present at the surface of strut-adjacent ECs.

FD surface modification has recently been proposed to improve hemocompatibility. Medtronic (Irvine, CA) has developed a phosphorylcholine surface modification of the Pipeline Embolization Device, with promising results regarding thrombogenicity,[25] neointimal hyperplasia, and endothelialization.[26,27] Manning et al[28] recently published a clinical series using the surface-modified FD (Pipeline Flex with Shield Technology, Medtronic). In this retrospective series, 14 ruptured intracranial aneurysms were treated in the acute phase after subarachnoid hemorrhage with the Pipeline Embolization Device–Shield under a single antiplatelet therapy. The authors reported 3 patients (21.4%) with thrombotic complications in the acute period, and two patients (14.3%) with rebleeding of the culprit aneurysm leading to patient death, pointing out the fact that these devices may not immediately prevent the risk of aneurysm rerupture. Such antithrombogenic coating may have an added value for specific aneurysms requiring an FD placement in the acute

phase after rupture. However, they represent a minority: <1% of intracranial aneurysms.[29] Furthermore, when an FD is used for unruptured aneurysms, the need for dual antiplatelet therapy does not carry a high ischemic risk,[30] and new antiplatelet treatments, such as ticagrelor or prasugrel, have been shown to reduce the occurrence of this complication.[31,32] CD31-mimetic coating strategy improves the global biological response by fostering arterial formation and aneurysmal occlusion and by reducing the thrombogenicity of the device. The latter property likely induces faster incorporation of the device in the arterial wall which is expected to shorten the period during which the struts remain exposed to reactive blood elements. This could lead to shorter periods of dual antiplatelet therapy and single antiplatelet therapy treatments after FD implantation. Our histopathology studies were performed at 4 weeks after FD implantation. It is possible however that some beneficial effects on histological healing could appear earlier.

Limitation of the Study

Further studies are required to evaluate the translational potential of our strategy on long-term preclinical studies. In the present study, the occlusion rate of CD31-FDs at 12 weeks tended to increase as compared to bare-FDs (100% versus 33%). However, the size of our preclinical study and the rabbit elastase model we used here were not intended to evaluate a difference in terms of aneurysmal occlusion but the effect of CD31-mimetic coating on FD endothelialization, which we consistently observed despite the small number of individuals analyzed. Although most studies in rabbit elastase aneurysm models use clopidogrel together with aspirin when testing FDs,[33] efficacy of the prodrug clopidogrel in rabbits has never been tested and a variable degree of resistance to clopidogrel occurs in patients (28 to 66%).[34,35] This explains why we used only aspirin and not a dual antiplatelet therapy to treat the experimental animals. Nonetheless, although clotting successfully failed to occur in the presence of CD31-mimetic coating, further studies are required before translation to clinical practice.

Conclusions

We demonstrated that CD31-mimetic coating can consistently improve endothelialization across the neck of arterial aneurysm implanted with FDs. The CD31-mimetic coating procedure evaluated in our study is simple and suitable for scaling-up and potential use in patients. Thus, CD31-mimetic coating appears as a promising strategy increasing FD biocompatibility, reducing body reactivity, and likely enhancing effective aneurysm healing. These results are a crucial step towards a translation to clinical use.

ARTICLE INFORMATION

Received May 5, 2020; final revision received September 30, 2020; accepted November 16, 2020.

Affiliations

NEURI Center, Hôpital Bicêtre, APHP–Université Paris Sud, Kremlin-Bicêtre, France (J. Cortese, J. Caroff, L.S.). Laboratory for Vascular Translational Science, Université de Paris, INSERM U1148, France (J. Cortese, C.R., G.E., C.C., J.M., A.N., J.-B.M., G.C.). Department of Interventional Neuroradiology, Limoges University Hospital, France (K.J., A.R.). University of Limoges, XLIM UMR CNRS 7252, France (S.M.B., M.-L.P., A.R.).

Acknowledgments

We thank Dr Melanie Gettings for critical reading and editing of the article, Dr Eric Largen (BALT Extrusion) for providing the flow diverters, and Claude Couquet (Plateforme MICE, Limoges, France) for his help and care with the animals.

Sources of Funding

This work was funded by the French National Research Agency (Agence Nationale de la Recherche [ANR]) Project IMPLANTS (ANR-14-CE17-0014), the Foundation for Medical Research (Fondation pour la Recherche Médicale [FRM]; DBS20140930764 to Dr Caligiuri) and (DEA20170637766 to Dr Cortese), the "Fondation de l'Avenir" (FA_CDC_AO_RMA_2013_Caligiuri), and from MSDAVENIR (Merck Sharp and Dohme Avenir, project "Save-Brain"). The ANR under the Investments for the future program also funded experiments on multiphoton imaging (ANR-10-LABX-0074-01 Sigma-LIM). Dr Cortese received a Grant from The French Society of Radiology (Société Française de Radiologie - Collège des Enseignants en Radiologie de France [SFR-CERF]) for this study.

Disclosures

Dr Nicoletti reports patent to PCT/FR2018/052991 pending. Dr Caligiuri reports patent to PCT/FR2018/052991 pending. Dr Mesnier reports personal fees from Owkin outside the submitted work. The other authors report no conflicts.

REFERENCES

1. Kallmes DF, Ding YH, Dai D, Kadirvel R, Lewis DA, Cloft HJ. A new endoluminal, flow-disrupting device for treatment of saccular aneurysms. *Stroke.* 2007;38:2346–2352. doi: 10.1161/STROKEAHA.106.479576
2. Kallmes DF, Brinjikji W, Cekirge S, Fiorella D, Hanel RA, Jabbour P, Lopes D, Lylyk P, McDougall CG, Siddiqui A. Safety and efficacy of the Pipeline embolization device for treatment of intracranial aneurysms: a pooled analysis of 3 large studies. *J Neurosurg.* 2017;127:775–780. doi: 10.3171/2016.8.JNS16467
3. Rouchaud A, Brinjikji W, Lanzino G, Cloft HJ, Kadirvel R, Kallmes DF. Delayed hemorrhagic complications after flow diversion for intracranial aneurysms: a literature overview. *Neuroradiology.* 2016;58:171–177. doi: 10.1007/s00234-015-1615-4
4. Gory B, Berge J, Bonafé A, Pierot L, Spelle L, Piotin M, Biondi A, Cognard C, Mounayer C, Sourour N, et al; DIVERSION Investigators. Flow diverters for intracranial aneurysms: the DIVERSION national prospective cohort study. *Stroke.* 2019;50:3471–3480. doi: 10.1161/STROKEAHA.119.024722
5. Kulcsár Z, Houdart E, Bonafé A, Parker G, Millar J, Goddard AJ, Renowden S, Gál G, Turowski B, Mitchell K, et al. Intra-aneurysmal thrombosis as a possible cause of delayed aneurysm rupture after flow-diversion treatment. *AJNR Am J Neuroradiol.* 2011;32:20–25. doi: 10.3174/ajnr.A2370
6. Cebral J, Ollikainen E, Chung BJ, Mut F, Sippola V, Jahromi BR, Tulamo R, Hernesniemi J, Niemelä M, Robertson A, et al. Flow conditions in the intracranial aneurysm lumen are associated with inflammation and degenerative changes of the aneurysm wall. *AJNR Am J Neuroradiol.* 2017;38:119–126. doi: 10.3174/ajnr.A4951
7. Skukalek SL, Winkler AM, Kang J, Dion JE, Cawley CM, Webb A, Dannenbaum MJ, Schuette AJ, Asbury B, Tong FC. Effect of antiplatelet therapy and platelet function testing on hemorrhagic and thrombotic complications in patients with cerebral aneurysms treated with the pipeline embolization device: a review and meta-analysis. *J Neurointerv Surg.* 2016;8:58–65. doi: 10.1136/neurintsurg-2014-011145
8. Ravindran K, Casabella AM, Cebral J, Brinjikji W, Kallmes DF, Kadirvel R. Mechanism of action and biology of flow diverters in the treatment of intracranial aneurysms. *Neurosurgery.* 2020;86(suppl 1):S13–S19. doi: 10.1093/neuros/nyz324

9. Giannotta M, Trani M, Dejana E. VE-cadherin and endothelial adherens junctions: active guardians of vascular integrity. *Dev Cell.* 2013;26:441–454. doi: 10.1016/j.devcel.2013.08.020
10. Marelli-Berg FM, Clement M, Mauro C, Caligiuri G. An immunologist's guide to CD31 function in T-cells. *J Cell Sci.* 2013;126(pt 11):2343–2352. doi: 10.1242/jcs.124099
11. Caligiuri G. Mechanotransduction, immunoregulation, and metabolic functions of CD31 in cardiovascular pathophysiology. *Cardiovasc Res.* 2019;115:1425–1434. doi: 10.1093/cvr/cvz132
12. Andreata F, Syvannarath V, Clement M, Delbosc S, Guedj K, Fornasa G, Khallou-Laschet J, Morvan M, Even G, Procopio E, et al. Macrophage CD31 signaling in dissecting aortic aneurysm. *J Am Coll Cardiol.* 2018;72:45–57. doi: 10.1016/j.jacc.2018.04.047
13. Ding YH, Floren M, Tan W. Mussel-inspired polydopamine for bio-surface functionalization. *Biosurf Biotribol.* 2016;2:121–136. doi: 10.1016/j.bsbt.2016.11.001
14. Manova RK, Pujari SP, Weijers CA, Zuilhof H, van Beek TA. Copper-free click biofunctionalization of silicon nitride surfaces via strain-promoted alkyne-azide cycloaddition reactions. *Langmuir.* 2012;28:8651–8663. doi: 10.1021/la300921e
15. Altes TA, Cloft HJ, Short JG, DeGast A, Do HM, Helm GA, Kallmes DF. Creation of saccular aneurysms in the rabbit. *Am J Roentgenol.* 2000;174:349–354.
16. Wegner KA, Keikhosravi A, Eliceiri KW, Vezina CM. Fluorescence of picrosirius red multiplexed with immunohistochemistry for the quantitative assessment of collagen in tissue sections. *J Histochem Cytochem.* 2017;65:479–490. doi: 10.1369/0022155417718541
17. Bardet SM, Cortese J, Blanc R, Mounayer C, Rouchaud A. Multiphoton microscopy for preclinical evaluation of flow-diverter stents for treating aneurysms [published online March 20, 2020]. *J Neuroradiol.* 2020:S0150-9861(20)30133-4. doi: 10.1016/j.neurad.2020.03.005
18. Lertkiatmongkol P, Liao D, Mei H, Hu Y, Newman PJ. Endothelial functions of platelet/endothelial cell adhesion molecule-1 (CD31). *Curr Opin Hematol.* 2016;23:253–259. doi: 10.1097/MOH.0000000000000239
19. Kadirvel R, Ding YH, Dai D, Rezek I, Lewis DA, Kallmes DF. Cellular mechanisms of aneurysm occlusion after treatment with a flow diverter. *Radiology.* 2014;270:394–399. doi: 10.1148/radiol.13130796
20. Coutard M, Touat Z, Houard X, Leclercq A, Michel JB. Thrombus versus wall biological activities in experimental aortic aneurysms. *J Vasc Res.* 2010;47:355–366. doi: 10.1159/000265569
21. Houard X, Rouzet F, Touat Z, Philippe M, Dominguez M, Fontaine V, Sarda-Mantel L, Meulemans A, Le Guludec D, Meilhac O, et al. Topology of the fibrinolytic system within the mural thrombus of human abdominal aortic aneurysms. *J Pathol.* 2007;212:20–28. doi: 10.1002/path.2148
22. D'Urso PI, Lanzino G, Cloft HJ, Kallmes DF. Flow diversion for intracranial aneurysms. *Stroke.* 2011;42:2363–2368.
23. Yang Z, Tu Q, Zhu Y, Luo R, Li X, Xie Y, Maitz MF, Wang J, Huang N. Mussel-inspired coating of polydopamine directs endothelial and smooth muscle cell fate for re-endothelialization of vascular devices. *Adv Healthc Mater.* 2012;1:548–559. doi: 10.1002/adhm.201200073
24. Perez DM. Structure-function of alpha1-adrenergic receptors. *Biochem Pharmacol.* 2007;73:1051–1062. doi: 10.1016/j.bcp.2006.09.010
25. Hagen MW, Girdhar G, Wainwright J, Hinds MT. Thrombogenicity of flow diverters in an ex vivo shunt model: effect of phosphorylcholine surface modification. *J Neurointerv Surg.* 2017;9:1006–1011. doi: 10.1136/neurintsurg-2016-012612
26. Caroff J, Tamura T, King RM, Lylyk PN, Langan ET, Brooks OW, Clarençon F, Wainwright JM, Spelle L, Marosfoi M, et al. Phosphorylcholine surface modified flow diverter associated with reduced intimal hyperplasia. *J Neurointerv Surg.* 2018;10:1097–1101. doi: 10.1136/neurintsurg-2018-013776
27. Matsuda Y, Jang DK, Chung J, Wainwright JM, Lopes D. Preliminary outcomes of single antiplatelet therapy for surface-modified flow diverters in an animal model: analysis of neointimal development and thrombus formation using OCT. *J Neurointerv Surg.* 2019;11:74–79. doi: 10.1136/neurintsurg-2018-013935
28. Manning NW, Cheung A, Phillips TJ, Wenderoth JD. Pipeline shield with single antiplatelet therapy in aneurysmal subarachnoid haemorrhage: multicentre experience. *J Neurointerv Surg.* 2019;11:694–698. doi: 10.1136/neurintsurg-2018-014363
29. Abe M, Tabuchi K, Yokoyama H, Uchino A. Blood blisterlike aneurysms of the internal carotid artery. *J Neurosurg.* 1998;89:419–424. doi: 10.3171/jns.1998.89.3.0419
30. Pikis S, Mantziaris G, Mamalis V, Barkas K, Tsanis A, Lyra S, Karkoulias K, Petrosyan T, Archontakis E. Diffusion weighted image documented cerebral ischemia in the postprocedural period following pipeline embolization device with shield technology treatment of unruptured intracranial aneurysms: a prospective, single center study. *J Neurointerv Surg.* 2020;12:407–411. doi: 10.1136/neurintsurg-2019-015363
31. Choi HH, Lee JJ, Cho YD, Han MH, Cho WS, Kim JE, An SJ, Mun JH, Yoo DH, Kang HS. Antiplatelet premedication for stent-assisted coil embolization of intracranial aneurysms: low-dose prasugrel vs clopidogrel. *Neurosurgery.* 2018;83:981–988. doi: 10.1093/neuros/nyx591
32. Soize S, Foussier C, Manceau PF, Litré CF, Backchine S, Gawlitza M, Pierot L. Comparison of two preventive dual antiplatelet regimens for unruptured intracranial aneurysm embolization with flow diverter/disrupter: a matched-cohort study comparing clopidogrel with ticagrelor. *J Neuroradiol.* 2019;46:378–383. doi: 10.1016/j.neurad.2019.01.094
33. Fahed R, Raymond J, Ducroux C, Gentric JC, Salazkin I, Ziegler D, Gevry G, Darsaut TE. Testing flow diversion in animal models: a systematic review. *Neuroradiology.* 2016;58:375–382. doi: 10.1007/s00234-015-1635-0
34. Uchiyama S. Clopidogrel resistance: identifying and overcoming a barrier to effective antiplatelet treatment. *Cardiovasc Ther.* 2011;29:e100–e111. doi: 10.1111/j.1755-5922.2010.00202.x
35. Fifi JT, Brockington C, Narang J, Leesch W, Ewing SL, Bennet H, Berenstein A, Chong J. Clopidogrel resistance is associated with thromboembolic complications in patients undergoing neurovascular stenting. *AJNR Am J Neuroradiol.* 2013;34:716–720. doi: 10.3174/ajnr.A3405